

# 3-dimensional distribution of spin-polarized current: application to (Cu/Co) pillar structures

J. Hamrle,<sup>1,2</sup> T. Kimura,<sup>1,2</sup> T. Yang,<sup>1,2</sup> and Y. Otani<sup>1,2,3</sup>

<sup>1</sup> FRS, The Institute of Physical and Chemical Research (RIKEN), 2-1 Hirosawa, Wako, Saitama 351-0198, Japan

<sup>2</sup>CREST, Japan Science & Technology Corporation, Japan

<sup>3</sup>ISSP, University of Tokyo, Kashiwa-shi, Chiba 277-8581, Japan

(Dated: November 10, 2018)

We present a formalism determining spin-polarized current and electrochemical potential inside arbitrary electric circuit within diffusive regime for parallel/antiparallel magnetic states. When arbitrary nano-structure is expressed by 3-dimensional (3D) electric circuit, we can determine 3D spin-polarized current and electrochemical potential distributions inside it. We apply this technique to (Cu/Co) pillar structures, where pillar is terminated either by infinitely large Cu layer, or by Cu wire with identical cross-sectional area as pillar itself. We found that infinitely large Cu layers work as a strong spin-scatterers, increasing magnitude of spin-polarized current inside the pillar twice and reducing spin accumulation nearly to zero. As most experimentally studied pillar structures are terminated by such a infinitely large layers, we propose modification of standard Valet-Fert formalism to simply include influence of such infinitely large layers.

PACS numbers: 75.75.+a, 85.70.Kh, 85.70.Ay

## I. INTRODUCTION

Spin injection, transport, and detection are key factors in the field of magnetoelectronics. Especially, magnetization reversal using spin-polarized current is of great interest [1, 2, 3, 4, 5, 6, 7] due to its potential technological applications such as MRAM [8], spin transistor [9] or spin battery [10].

To understand and optimize spin-transport behavior in such devices, it is important to know a current distribution in it. Particularly for MRAM applications, we have to know spin-current magnitude and distribution to optimize the current density necessary for spin-injection induced magnetization reversal. Variety of formalisms calculating magnetoelectronic transport in one dimension (1D) even for non-collinear magnetization has been proposed [11, 12, 13, 14, 15].

However, up to now, the spatial (3D) calculation of the spin-polarized current have been missing. To obtain spatial distribution of spin-polarized current (and spin accumulation) in a given structure, we express such a structure as a 3D circuit of spin-dependent-resistor-elements (SDRE), wherein the propagation is regarded as 1D problem [11, 16].

Resistor circuit network has been already used in [17] to simulate current lines in metal/insulator multilayers. However, in this case, they did not use spin-polarized current. Ichimura et al. [18] have calculated 2D distribution of spin polarized current for Co/Al lateral spin valve structure. They did not use the electric circuit, but directly solved Poisson equation by means of finite element method.

This article is organized as follows: Sections II and II A present a matrix approach to calculate 1D diffusive propagation of spin-polarized current and potential in the single SDRE. Section II B shows how this formalism can be applied to a simple multilayer structure. This

approach is just compact matrix rewriting the 1D Valet-Fert (VF) formalism [11]. Section III explains how to solve general electric circuit and Section III A tells how to divide nanostructure into circuit of SDREs. Finally, in Section IV we apply our calculations to (Cu/Co)<sup>2</sup>, and (Cu/Co)<sup>3</sup> pillar structures, where cross-sectional areas of the first and last layers are assumed either the same as the pillar, or infinitely large. We show how the presence of such infinitely large layers influence currents and spin accumulation profiles. Finally Section V shows how to modify VF formalism to describe influence of the infinitely large layers.

## II. DIFFUSIVE TRANSPORT REGIME

In the diffusive transport regime, equations deriving the spatial distribution of electrochemical potential  $\mu_{\uparrow/\downarrow}$  and spin-polarized current density  $j_{\uparrow/\downarrow}$  inside ferro or non-magnetic metals are [11, 16, 19, 20]

$$\nabla^2(\mu_{\uparrow} - \mu_{\downarrow}) = \frac{\mu_{\uparrow} - \mu_{\downarrow}}{\lambda^2}, \quad (1)$$

$$j_{\uparrow/\downarrow} = -\frac{\sigma_{\uparrow/\downarrow}}{e} \nabla \mu_{\uparrow/\downarrow}, \quad (2)$$

where  $\lambda$  is spin-flip diffusion length,  $\sigma_{\uparrow/\downarrow} = \sigma(1 \pm \beta)/2$  conductivities for up and down channels, respectively and  $e$  the electron charge assumed to be  $e = 1$  in this article.

Our model is based on the circuit of SDRE, consisting of layers and interfaces (Fig. 1). We first express response of a single layer. When Eqs. (1)(2) are solved in 1D, the profiles of  $\mu_{\uparrow}$  and  $\mu_{\downarrow}$  (hereafter denoted as  $\mu_{\uparrow/\downarrow}$ ) inside

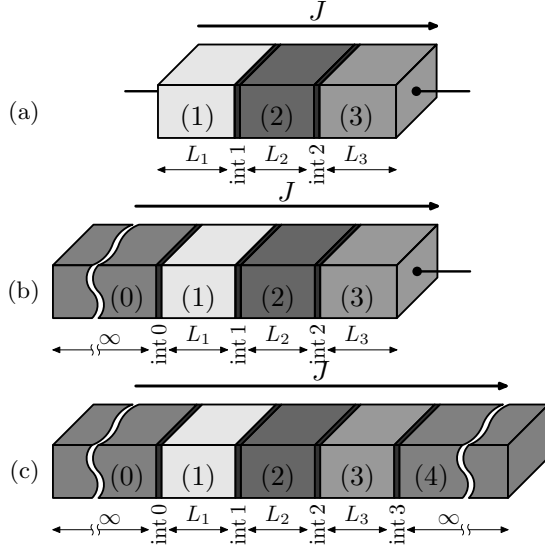


FIG. 1: A general form of (a) close-end SDRE (b) open-end SDRE (c) classical multilayer structure having both ends open-ended. The arrow shows positive both structure and current direction. In all cases, SDRE has three layers,  $M = 3$ .

a given material along  $x$ -axis is given by [11, 16]

$$\begin{aligned} \mu_{\uparrow/\downarrow}(x + L) &= \tilde{\mu}(x) + \frac{j_{\text{ch}}e}{\sigma}L \pm c(x)\frac{\sigma}{\sigma_{\uparrow/\downarrow}} \exp[-L/\lambda] \\ &\quad \pm d(x)\frac{\sigma}{\sigma_{\uparrow/\downarrow}} \exp[L/\lambda], \end{aligned} \quad (3)$$

where  $j_{\text{ch}} = j_{\uparrow} + j_{\downarrow}$  is charge current density and positive current direction is towards positive  $x$ -direction. Energies  $c(x)$  and  $d(x)$  are amplitudes of exponential damping of  $\mu_{\uparrow/\downarrow}$  and the energy  $\tilde{\mu}(x)$  is the asymptotic electrochemical potential equivalent to weighted average of electrochemical potentials  $\tilde{\mu} = (\sigma_{\uparrow}\mu_{\uparrow} + \sigma_{\downarrow}\mu_{\downarrow})/\sigma$ . The energies  $\tilde{\mu}$ ,  $c$  and  $d$  will be determined later from boundary conditions.

The relation between  $\mu_{\uparrow/\downarrow}$ ,  $j_{\uparrow/\downarrow}$  and  $\tilde{\mu}$ ,  $c$ ,  $d$  used in Eqs. (2) and (3) can be expressed in a compact matrix form

$$\begin{bmatrix} \mu_{\uparrow} \\ \mu_{\downarrow} \\ uJ_{\uparrow} \\ uJ_{\downarrow} \end{bmatrix}_x = \begin{bmatrix} 1 & \frac{\sigma}{\sigma_{\uparrow}} & \frac{\sigma}{\sigma_{\downarrow}} & 0 \\ 1 & -\frac{\sigma}{\sigma_{\downarrow}} & -\frac{\sigma}{\sigma_{\uparrow}} & 0 \\ 0 & -\frac{u\sigma S}{e\lambda} & \frac{u\sigma S}{e\lambda} & \frac{\sigma_{\uparrow}}{\sigma_{\downarrow}} \\ 0 & \frac{u\sigma S}{e\lambda} & -\frac{u\sigma S}{e\lambda} & \frac{\sigma_{\downarrow}}{\sigma_{\uparrow}} \end{bmatrix} \cdot \begin{bmatrix} \tilde{\mu} \\ c \\ d \\ uJ_{\text{ch}} \end{bmatrix}_x \quad (4)$$

where  $J_{\uparrow/\downarrow} = Sj_{\uparrow/\downarrow}$  is up/down spin-polarized current with cross-section area  $S$  of a given layer,  $J_{\text{ch}} = J_{\uparrow} + J_{\downarrow}$  is a charge current flowing through layer. The scaling factor  $u$  which has no physical meaning, is introduced to adjust units of newly defined  $\mathbf{H}$  and  $\mathbf{F}$  vectors. For numerical calculations, value of  $u$  should adjust order of  $\mu_{\uparrow/\downarrow}$  and  $uJ_{\uparrow/\downarrow}$ . When expressing any measurable quantities (e.g.  $\mu_{\uparrow/\downarrow}$ ,  $J_{\uparrow/\downarrow}$ , resistances), they obviously do not depend on  $u$ .

The left side of Eq. (4) ( $\mathbf{H}$ -vector) contains variables, which are conserved across interfaces or electric nodes. On the other hand, the right side of Eq. (4) ( $\mathbf{F}$ -vector) contains variables, which are used to calculate propagation of the  $J_{\uparrow/\downarrow}$  and  $\mu_{\uparrow/\downarrow}$  through layers [Eq. (3)]. Hence, the dynamic  $\mathbf{D}$ -matrix relates coefficients at the boundary to coefficients for propagation. This approach is well-known in the optics of anisotropic media [21, 22].

Propagation of  $\mathbf{F}$ -vector through layer with the thickness (“length”)  $L$  is expressed by a propagation  $\mathbf{P}$ -matrix [Eq.(3)]

$$\begin{bmatrix} \tilde{\mu} \\ c \\ d \\ uJ_{\text{ch}} \end{bmatrix}_{x+L} = \begin{bmatrix} 1 & 0 & 0 & \frac{ue}{\sigma S}L \\ 0 & e^{-L/\lambda} & 0 & 0 \\ 0 & 0 & e^{L/\lambda} & 0 \\ 0 & 0 & 0 & 1 \end{bmatrix} \cdot \begin{bmatrix} \tilde{\mu} \\ c \\ d \\ uJ_{\text{ch}} \end{bmatrix}_x \quad (5)$$

Hence, the relation between  $\mathbf{H} = [\mu_{\uparrow}, \mu_{\downarrow}, uJ_{\uparrow}, uJ_{\downarrow}]$  at both ends of the layer is expressed as

$$\mathbf{H}_x = \mathbf{D}\mathbf{P}\mathbf{D}^{-1}\mathbf{H}_{x+L} = \mathbf{K}\mathbf{H}_{x+L}. \quad (6)$$

### A. Interface resistivity and shunting interface resistance

In the previous Section, we have expressed response of one layer in homogeneous material. Here, we describe the interfacial properties including (i) interface resistance [11]  $AR_{\uparrow/\downarrow} = 2AR^*(1 \mp \gamma)$  and (ii) interfacial spin-flip scattering, described by a shunting resistance  $AR_s$ , “shortcircuiting” up and down channels at the interface. The response of interface can be expressed by  $\mathbf{K}_{\text{int}}$  matrix

$$\mathbf{H}_{x-dx} = \mathbf{K}_{\text{int}}\mathbf{H}_{x+dx}, \quad (7)$$

where  $x \mp dx$  denotes for  $\mathbf{H}$ -vector just below/above interface and  $\mathbf{K}_{\text{int}}$  writes

$$\mathbf{K}_{\text{int}} = \begin{bmatrix} 1 & 0 & -\frac{AR_{\uparrow}}{uS} & 0 \\ 0 & 1 & 0 & -\frac{AR_{\downarrow}}{uS} \\ -\frac{uS}{AR_s} & \frac{uS}{AR_s} & 1 & 0 \\ \frac{uS}{AR_s} & -\frac{uS}{AR_s} & 0 & 1 \end{bmatrix}. \quad (8)$$

Notice that alternative interfacial spin-flip scattering by  $\delta_I$ -parameter was introduced in [23, 24] describing spin relaxation at the interfaces by a thin interfacial layer of spin-flip-length  $\lambda_I = t_I/\delta_I$  where  $t_I$  is interfacial layer thickness. From comparison of  $\mathbf{K}$ -matrices from Eqs.(6) and (8),  $AR_s = 4t_I/(\sigma_I\delta_I^2)\sinh\delta_I$  where  $t_I$  and  $\sigma_I$  are interfacial layer thickness and conductivity, respectively. When interfacial spin-flip scattering does not exist, then  $R_s = \infty$ .

### B. Simple multilayer structure

Although the formalism developed here is mainly to calculate  $\mu_{\uparrow/\downarrow}$ ,  $j_{\uparrow/\downarrow}$  inside an electrical circuit, we shall

first show how presented  $4 \times 4$  matrix algebra can be used to calculate electrical response of a multilayer structure [Fig. 1(c)].

The description for a single layer by matrix  $\mathbf{K}$  in Eq. (6) gives relationship between  $\mu_{\uparrow/\downarrow}$  and  $J_{\uparrow/\downarrow}$  at both ends of the layer. Hereafter, instead of continuity of spin-polarized current density  $j_{\uparrow/\downarrow}$  over interface, we consider continuity of spin-polarized current  $J_{\uparrow/\downarrow}$ , to take into account variable cross-sectional area  $S$  of layers. The reasons and validity are discussed later in Section V. Obviously, when all layers have the same  $S$ , our formalism provides the same results as original VF formalism [11].

The boundary conditions at interfaces are continuity of  $\mu_{\uparrow/\downarrow}$  and  $J_{\uparrow/\downarrow}$ , i.e. continuity of  $\mathbf{H}$ -vector. Consequently, the response of whole multilayer structure can be written as [21, 22]

$$\mathbf{F}^{(0)} = \mathbf{M}^{(M+1)} \cdot \mathbf{F}^{(M+1)}, \quad (9)$$

where

$$\begin{aligned} \mathbf{M}^{(M+1)} = & [\mathbf{D}^{(0)}]^{-1} \mathbf{K}_{\text{int}}^{(0)} \mathbf{K}_{\text{int}}^{(1)} \mathbf{K}_{\text{int}}^{(1)} \dots \\ & \mathbf{K}_{\text{int}}^{(M-1)} \mathbf{K}_{\text{int}}^{(M)} \mathbf{K}_{\text{int}}^{(M)} \mathbf{D}^{(M+1)} \end{aligned} \quad (10)$$

where upper index in parenthesis denotes for interface or layer number,  $M$  the number of layers.

Because materials (0) and ( $M+1$ ) are semi-infinite,  $\mu_{\uparrow/\downarrow}$  inside them must not exponentially increase. Hence, some exponential terms in Eq. (3) must vanish, namely  $c^{(0)} \equiv 0$ ,  $d^{(M+1)} \equiv 0$ . Hence, the vectors  $\mathbf{F}^{(0)}$  and  $\mathbf{F}^{(M+1)}$  are limited to form

$$\mathbf{F}^{(0)} = \begin{bmatrix} \tilde{\mu}^{(0)} \\ 0 \\ d^{(0)} \\ uJ_{\text{ch}} \end{bmatrix} \quad \mathbf{F}^{(M+1)} = \begin{bmatrix} \tilde{\mu}^{(M+1)} \\ c^{(M+1)} \\ 0 \\ uJ_{\text{ch}} \end{bmatrix}. \quad (11)$$

Now, Eq.(9) can be solved. Substituting Eq. (11) to Eq. (9), we found all unknowns in  $\mathbf{F}^{(M+1)}$

$$\begin{bmatrix} \tilde{\mu}^{(M+1)} \\ c^{(M+1)} \end{bmatrix} = \left( \begin{bmatrix} M_{11} & M_{12} \\ M_{21} & M_{22} \end{bmatrix} \right)^{-1} \cdot \begin{bmatrix} -uM_{14}J_{\text{ch}} + \tilde{\mu}^{(0)} \\ -uM_{24}J_{\text{ch}} \end{bmatrix}, \quad (12)$$

where  $M_{ij}$  are elements of  $\mathbf{M}$ -matrix. The value of  $\tilde{\mu}^{(0)}$  can be arbitrary value, as it only adds a constant to the profiles of  $\mu_{\uparrow/\downarrow}$ . Other simplification of Eq. (12) follow from  $M_{11} \equiv 1$  and  $M_{21} \equiv 0$ , in consequence of (i) for  $J_{\text{ch}} = 0$  the terms  $\mu_{\uparrow/\downarrow}$ ,  $\tilde{\mu}$  must be constant and equal to each other and (ii) for  $J_{\text{ch}} = 0$ ,  $c^{(M+1)} = 0$ . Then, solution of Eq. (12) can be written as

$$\begin{aligned} \tilde{\mu}^{(M+1)} - \tilde{\mu}^{(0)} &= \left( -M_{14} + \frac{M_{12}M_{24}}{M_{22}} \right) uJ_{\text{ch}} \\ c^{(M+1)} &= -\frac{M_{24}}{M_{22}} uJ_{\text{ch}}. \end{aligned} \quad (13)$$

Now,  $\tilde{\mu}^{(M+1)}$  and  $c^{(M+1)}$  are known and therefore the vector  $\mathbf{F}^{(M+1)}$  can be reconstructed from Eq. (11). Consequently, the profiles of  $\mu_{\uparrow/\downarrow}$ ,  $\tilde{\mu}$ ,  $J_{\uparrow/\downarrow}$  etc. in the entire

structure can be determined by recursive applying step-by-step matrix multiplications in Eq. (10)

Finally, resistivity of the multilayer structure (between first and last interface) is  $R = (\tilde{\mu}^{(M+1)} - \tilde{\mu}^{(0)})/J_{\text{ch}}$ .

### III. ELECTRIC CIRCUIT

As demonstrated in the previous Section, the  $\mathbf{M}$ -matrix [defined by Eq. (9)] can characterize the entire multilayer structure where the same charge current  $J_{\text{ch}}$  flows across all layers. In this Section, we extend the previous formalism to an electrical circuit (network) of SDREs, mutually connected at nodes. In general, the SDRE is composed of any sequence of materials (layers) and/or interfaces, as depicted on Fig. 1. There are three types of SDRE, depending whether the length of SDRE is finite or infinite:

- close-end SDRE [Fig. 1(a)] has finite length and hence both ends of this SDRE are attached to nodes. Because the boundary condition at nodes are described by  $\mathbf{H}$ -vectors, whole SDRE is described by  $\mathbf{K}^{[b]}$ -matrix relating  $\mathbf{H}$ -vectors at both ends of SDRE:

$$\mathbf{H}^{[b](0)} = \mathbf{K}^{[b]} \mathbf{H}^{[b](M_b)}, \quad (14)$$

where, for later purpose,  $\mathbf{K}^{[b]}$  can be rewritten into four  $2 \times 2$  submatrices

$$\begin{bmatrix} \boldsymbol{\mu} \\ u\mathbf{J} \end{bmatrix}^{[b](0)} = \begin{bmatrix} \mathbf{K}_{\mu\mu} & \mathbf{K}_{\mu J} \\ \mathbf{K}_{J\mu} & \mathbf{K}_{JJ} \end{bmatrix}^{[b]} \begin{bmatrix} \boldsymbol{\mu} \\ u\mathbf{J} \end{bmatrix}^{[b](M_b)}, \quad (15)$$

where  $b$  denotes a SDRE number in the circuit and  $M_b$  is the number of layers in  $b$ -th SDRE,  $\boldsymbol{\mu}^{[b](M_b)} \equiv [\mu_{\uparrow}^{[b](M_b)}, \mu_{\downarrow}^{[b](M_b)}]^T$  and  $\mathbf{J}^{[b](M_b)} \equiv [J_{\uparrow}^{[b](M_b)}, J_{\downarrow}^{[b](M_b)}]^T$ ,  $T$  denoting vector transposition. Hereafter, indices in square bracket denotes for SDRE number, whereas indices in ordinary parentheses denotes for number of layer inside SDRE. Positive current direction is from layer (1) to layer ( $M_b$ ). Analogous to Eq. (10),  $\mathbf{K}^{[b]}$  consists of layer and interface contributions

$$\mathbf{K}^{[b]} = \mathbf{K}^{[b](1)} \mathbf{K}_{\text{int}}^{[b](1)} \dots \mathbf{K}_{\text{int}}^{[b](M_b-1)} \mathbf{K}^{[b](M_b)}. \quad (16)$$

When SDRE contains only one layer (i.e. it consists of single metal), then [Eq. (6)]  $\mathbf{K}^{[b]} = \mathbf{K}^{[b](1)} \equiv \mathbf{D}^{[b]} \mathbf{P}^{[b]} [\mathbf{D}^{[b]}]^{-1}$ .

- open-end SDRE [Fig. 1(b)] has one end “finite” and connected to the node. The other end is infinitely long and at its end the charge current  $J_{\text{ch}}^{[b](0)}$ , flowing into the  $b$ -th open-end SDRE, is applied. Because boundary conditions on node are described by  $\mathbf{H}$ -vector and boundary conditions of the propagation into infinity by  $\mathbf{F}$ -vector, the  $b$ -th open-end

SDRE is described by  $\mathbf{Z}^{[b]}$ -matrix as

$$\mathbf{F}^{[b](0)} = \mathbf{Z}^{[b]} \mathbf{H}^{[b](M_b)}, \quad (17)$$

where we have used convention that direction of SDRE and positive current direction goes from infinite end of SDRE toward its finite end [Fig. 1(b)]. Analogous to Eqs. (10) and (16)

$$\mathbf{Z}^{[b]} = [\mathbf{D}^{[b](0)}]^{-1} \mathbf{K}_{\text{int}}^{[b](0)} \mathbf{K}^{[b](1)} \mathbf{K}_{\text{int}}^{[b](1)} \dots \mathbf{K}_{\text{int}}^{[b](M_b-1)} \mathbf{K}^{[b](M_b)}. \quad (18)$$

When the SDRE contains no layer (i.e. it contains only single material continuous to infinity), then  $\mathbf{Z}^{[b]} = [\mathbf{D}^{[b]}]^{-1}$ .

- multilayer structure [Fig. 1(c)] described in Sect. II B may be understood as a special type of SDRE, having both ends open-ended.

In general, the electric circuit is assumed to have  $N$  nodes,  $C$  close-end SDRE and  $E$  open-end SDRE.

The boundary conditions valid for each node are determined by generalized Kirchoff's laws:

$$\mu_{n,\uparrow/\downarrow}^{[b_n]} = \text{const}_{n,\uparrow/\downarrow} \equiv \mu_{n,\uparrow/\downarrow}, \quad (19)$$

$$\sum_{b_n=1}^{B_n} J_{n,\uparrow/\downarrow}^{[b_n]} = 0, \quad (20)$$

i.e. the values of  $\mu_{\uparrow/\downarrow}$  has to be identical for all ends of SDRE connected to each node and sum of polarized currents  $J_{\uparrow/\downarrow}$  entering each node has to be zero. Subscript  $n$  denotes for node number,  $n = 1 \dots N$  and  $b_n = 1, \dots, B_n$  denotes the SDREs connected to the  $n$ -th node.

Hereafter, we use two  $\mu$ -notation (i)  $\mu_{n,\uparrow/\downarrow}$  relating  $\mu_{\uparrow/\downarrow}$  at the  $n$ -th node and (ii)  $\mu_{\uparrow/\downarrow}^{[b](0)}$ ,  $\mu_{\uparrow/\downarrow}^{[b](M_b)}$  denoting  $\mu_{\uparrow/\downarrow}$  at start, end of the  $b$ -th SDRE, respectively. The

relation between these two  $\mu$ -notations is given by connections between nodes and SDREs, i.e. by the topology of the electric circuit.

Following the previous discussion, the problem is how to treat large number of linear equations (14)(17)(19)(20) giving relations between  $\mu_{\uparrow/\downarrow}$  and  $J_{\uparrow/\downarrow}$  on the nodes and between ends of SDREs. We do it by solving one large matrix expression,

$$\mathbf{Q} \cdot \mathbf{H} = \mathbf{F}, \quad (21)$$

to which we apply all the previously mentioned rules. The  $\mathbb{H}$ -vector contains  $\mu_{n,\uparrow/\downarrow}$  for all nodes and also  $uJ_{\uparrow/\downarrow}^{[b](M_b)}$ ,  $b = 1 \dots C + E$ , at the *end* (i.e. at the  $M_b$ -side) of each SDRE. Hence,  $\mathbb{H}$ -vector has  $2(C + E + N)$  elements.

The role of the  $\mathbf{Q}$ -matrix consists of three parts [Eq.(22)]:

- (1) to relate  $\mu_{\uparrow/\downarrow}$ ,  $J_{\uparrow/\downarrow}$  at the “finite” end of the open-end SDREs and between boundary conditions of propagation towards infinity. This is provided by  $2E$  linear equation, and hence this part occupies  $2E$  rows in  $\mathbf{Q}$ -matrix.
- (2) to relate  $\mu_{\uparrow/\downarrow}$  between start and end of the close-end SDREs ( $2C$  linear equations).
- (3) to realize current conservation at each node ( $2N$  linear equations).

These contributions are studied in detail in following. In total,  $\mathbf{Q}$ -matrix has  $2(C + E + N)$  rows, the same as length of  $\mathbf{H}$ -vector. So  $\mathbf{Q}$  is a square matrix.

An example of a circuit of SDREs is depicted in Figure 2. The circuit consist of  $N = 3$  nodes, connected by SDRE. The circuit consists of  $C = 3$  close-end SDRE and  $E = 2$  open-end SDREs. Then, the resulting equation  $\mathbf{QH} = \mathbf{F}$  looks like:

$$\left[ \begin{array}{ccc|ccc|ccc} \tilde{\mathbf{Z}}_{\mu}^{[1]} & \mathbf{0} & \mathbf{0} & \tilde{\mathbf{Z}}_J^{[1]} & \mathbf{0} & \mathbf{0} & \mathbf{0} & \mathbf{0} & \mathbf{0} \\ \mathbf{0} & \mathbf{0} & \tilde{\mathbf{Z}}_{\mu}^{[5]} & \mathbf{0} & \mathbf{0} & \mathbf{0} & \mathbf{0} & \mathbf{0} & \tilde{\mathbf{Z}}_J^{[5]} \\ \hline -1 & \mathbf{K}_{\mu,\mu}^{[2]} & \mathbf{0} & \mathbf{0} & \mathbf{K}_{\mu J}^{[2]} & \mathbf{0} & \mathbf{0} & \mathbf{0} & \mathbf{0} \\ \mathbf{0} & -1 & \mathbf{K}_{\mu,\mu}^{[3]} & \mathbf{0} & \mathbf{0} & \mathbf{K}_{\mu J}^{[3]} & \mathbf{0} & \mathbf{0} & \mathbf{0} \\ -1 & \mathbf{0} & \mathbf{K}_{\mu,\mu}^{[4]} & \mathbf{0} & \mathbf{0} & \mathbf{0} & \mathbf{K}_{\mu J}^{[4]} & \mathbf{0} & \mathbf{0} \\ \hline \mathbf{0} & \mathbf{K}_{J\mu}^{[2]} & \mathbf{K}_{J\mu}^{[4]} & -1 & \mathbf{K}_{JJ}^{[2]} & \mathbf{0} & \mathbf{K}_{JJ}^{[4]} & \mathbf{0} & \mathbf{0} \\ \mathbf{0} & \mathbf{0} & \mathbf{K}_{J\mu}^{[3]} & \mathbf{0} & -1 & \mathbf{K}_{JJ}^{[3]} & \mathbf{0} & \mathbf{0} & \mathbf{0} \\ \mathbf{0} & \mathbf{0} & \mathbf{0} & \mathbf{0} & \mathbf{0} & -1 & -1 & -1 & -1 \end{array} \right] \left[ \begin{array}{c} \mu_1 \\ \mu_2 \\ \hline \mu_3 \\ uJ^{[1](M_1)} \\ uJ^{[2](M_2)} \\ uJ^{[3](M_3)} \\ uJ^{[4](M_4)} \\ uJ^{[5](M_5)} \end{array} \right] = \left[ \begin{array}{c} \tilde{\mathbf{F}}^{[1](0)} \\ \tilde{\mathbf{F}}^{[5](0)} \\ \hline \mathbf{0} \\ \mathbf{0} \\ \mathbf{0} \\ \mathbf{0} \\ \mathbf{0} \\ \mathbf{0} \end{array} \right] \quad (22)$$

where  $\boldsymbol{\mu}_n \equiv [\mu_{n,\uparrow}, \mu_{n,\downarrow}]^T$  and  $\mathbf{1}$ ,  $\mathbf{0}$  denote  $2 \times 2$  unitary, zero matrix, respectively. Each row which is shown in  $\mathbf{Q}$ -

matrix in Eq. (22) represents two rows (for up and down channel), so hereafter we call it “double-row”.

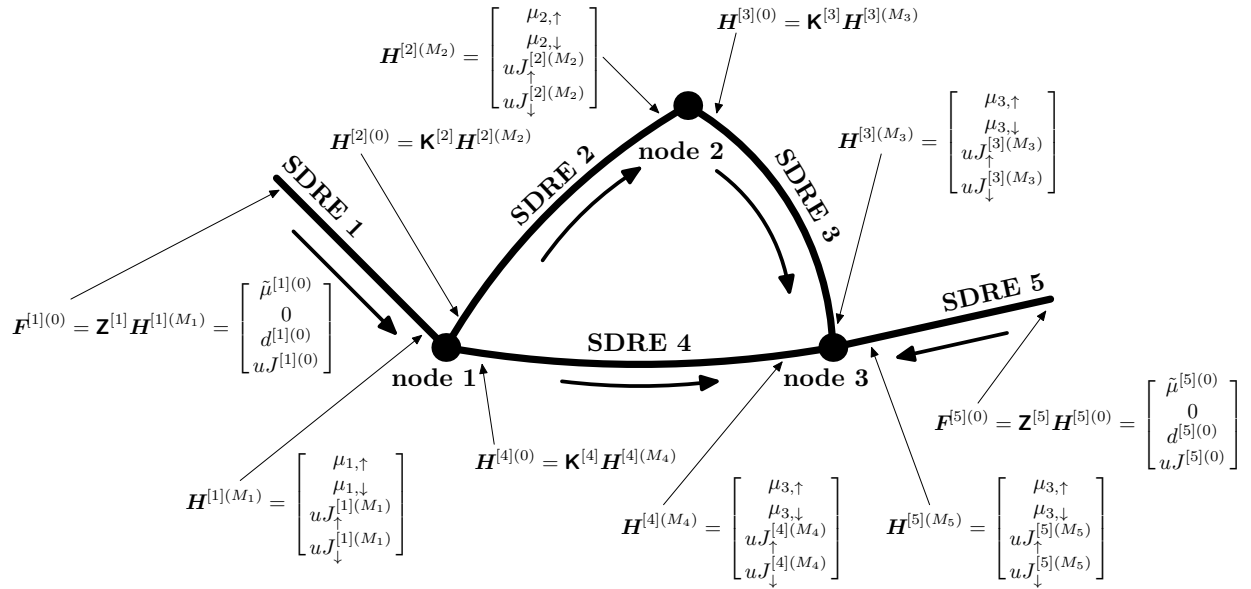


FIG. 2: The schema of a circuit example, consisting of three node, two open-end SDRE and three close-end SDRE. The arrows parallel to SDRE shows the defined direction of SDRE (and hence also positive current direction).

(ad 1) The role of the first part in the  $\mathbb{Q}$ -matrix relates both ends of open-end SDRE, described by Eq. (17),  $\mathbf{F}^{[b](0)} = \mathbf{Z}^{[b]} \mathbf{H}^{[b](M_b)}$ . However, we only know 2 variables out of 4 in vector  $\mathbf{F}^{[b](0)} = [\tilde{\mu}^{[b](0)}, c^{[b](0)}, d^{[b](0)}, uJ_{ch}^{[b](0)}]^T$ . We know charge current  $J_{ch}^{[b](0)}$  entering  $b$ -th SDRE and that  $c^{[b](0)} = 0$ , because  $\mu_{\uparrow/\downarrow}$  must not exponentially increase towards infinity [Eq. (11)]. Hence, taking from  $\mathbf{Z}^{[b]}$ -matrix [Eq.(17)] only rows corresponding with known value in  $\mathbf{F}^{[b](0)}$ , we get

$$\tilde{\mathbf{F}}^{[b](0)} \equiv \begin{bmatrix} 0 \\ uJ_{ch}^{[b](0)} \end{bmatrix} = \begin{bmatrix} Z_{21} & Z_{22} & Z_{23} & Z_{24} \\ Z_{41} & Z_{42} & Z_{43} & Z_{44} \end{bmatrix}^{[b]} \begin{bmatrix} \mu_{\uparrow} \\ \mu_{\downarrow} \\ uJ_{\uparrow} \\ uJ_{\downarrow} \end{bmatrix}^{[b](M_b)} \\ \equiv \begin{bmatrix} \tilde{\mathbf{Z}}_{\mu}^{[b]} & \tilde{\mathbf{Z}}_J^{[b]} \end{bmatrix} \begin{bmatrix} \boldsymbol{\mu}^{[b](M_b)} \\ u\mathbf{J}^{[b](M_b)} \end{bmatrix}. \quad (23)$$

This equation is substituted into first part of in  $\mathbb{Q}$ -matrix [Eq. (22)] in the form:  $\tilde{\mathbf{Z}}_{\mu}^{[b]} \boldsymbol{\mu}^{[b](M_b)} + \tilde{\mathbf{Z}}_J^{[b]} u\mathbf{J}^{[b](M_b)} = \tilde{\mathbf{F}}^{[b](0)}$ .

In the case of the last open-end SDRE connected to the structure (in our example SDRE number  $b' = 5$ ), the situation is slightly different. In the vector  $\mathbf{F}^{[b'](0)} = [\tilde{\mu}^{[b'](0)}, c^{[b'](0)}, d^{[b'](0)}, uJ_{ch}^{[b'](0)}]^T$  (a) we have to set a value of  $\tilde{\mu}^{[b'](0)}$ , which sets an absolute value of all  $\mu_{\uparrow/\downarrow}$  and  $\tilde{\mu}$  inside circuit to an arbitrary value and (b) getting a charge current  $J_{ch}^{[b'](0)}$  would be redundant as a sum of all charge currents entering circuit has to be zero. Hence, the last double-row in the first part of the  $\mathbb{Q}$ -matrix (sec-

ond double-row in Eq. (22)) looks like

$$\tilde{\mathbf{F}}'^{[b'](0)} \equiv \begin{bmatrix} \tilde{\mu}^{[b'](0)} \\ 0 \end{bmatrix} = \begin{bmatrix} Z_{11} & Z_{12} & Z_{13} & Z_{14} \\ Z_{21} & Z_{22} & Z_{23} & Z_{24} \end{bmatrix}^{[b']} \begin{bmatrix} \mu_{\uparrow} \\ \mu_{\downarrow} \\ uJ_{\uparrow} \\ uJ_{\downarrow} \end{bmatrix}^{[b'](M_b)} \\ \equiv \begin{bmatrix} \tilde{\mathbf{Z}}_{\mu}'^{[b']} & \tilde{\mathbf{Z}}_J'^{[b']} \end{bmatrix} \begin{bmatrix} \boldsymbol{\mu}^{[b'](M_b)} \\ u\mathbf{J}^{[b'](M_b)} \end{bmatrix} \quad (24)$$

and is substituted to  $\mathbb{Q}$ -matrix analogous as Eq. (23).

(ad 2) The second part in the  $\mathbb{Q}$ -matrix gives relation between  $\mu_{\uparrow/\downarrow}^{[b](0)}$  at the start of the  $b$ -th close-end SDRE and  $\mu_{\uparrow/\downarrow}^{[b](M_b)}$ ,  $J_{\uparrow/\downarrow}^{[b](M_b)}$  at the end of  $b$ -th SDRE. This relation is given by the first double row taken from Eq. (15). It is substituted into  $\mathbb{Q}$  in the form  $0 = -\boldsymbol{\mu}^{[b](0)} + \mathbf{K}_{\mu\mu}^{[b]} \boldsymbol{\mu}^{[b](M_b)} + u\mathbf{K}_{\mu J}^{[b]} \mathbf{J}^{[b](M_b)}$ .

(ad 3) The last part in  $\mathbb{Q}$ -matrix describes the current conservation at each node, described by Kirchoff's law Eq. (20). As specified,  $\mathbb{H}$ -vector contains only values of current at the end of each SDRE,  $J_{\uparrow/\downarrow}^{[b](M_b)}$ . Hence, if the  $b$ -th SDRE starts at the  $n$ -th node (as No. 2 and 4 SDREs at the node 1), then the current is expressed by the second double-row in Eq. (15), from  $\mu_{\uparrow/\downarrow}^{[b](M_b)}$ ,  $J_{\uparrow/\downarrow}^{[b](M_b)}$  as  $u\mathbf{J}^{[b](0)} = \mathbf{K}_{J\mu}^{[b]} \boldsymbol{\mu}^{[b](M_b)} + u\mathbf{K}_{JJ}^{[b]} \mathbf{J}^{[b](M_b)}$ . For example, in case of node  $n = 1$ , the current conservation is  $-J_{\uparrow/\downarrow}^{[1](M_1)} + J_{\uparrow/\downarrow}^{[2](0)} + J_{\uparrow/\downarrow}^{[4](0)} = 0$ , which is substituted to  $\mathbb{Q}$ -matrix to the 6-th double-row as  $-\mathbf{J}^{[1](M_1)} + \mathbf{K}_{J\mu}^{[2]} \boldsymbol{\mu}^{[2](M_2)} + u\mathbf{K}_{JJ}^{[2]} \mathbf{J}^{[2](M_2)} + \mathbf{K}_{J\mu}^{[4]} \boldsymbol{\mu}^{[4](M_4)} + u\mathbf{K}_{JJ}^{[4]} \mathbf{J}^{[4](M_4)} = \mathbf{0}$ .

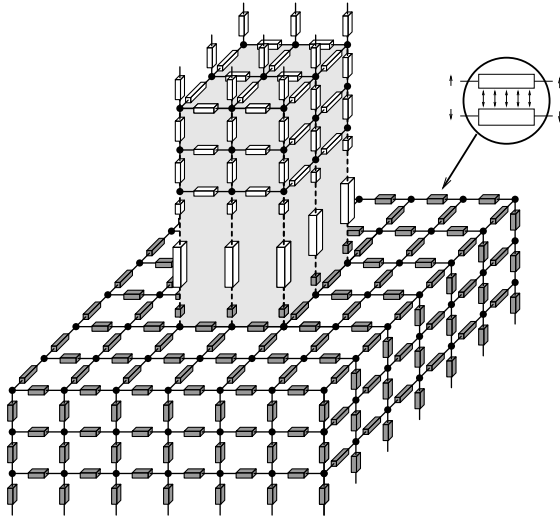


FIG. 3: An example of dividing nanostructure into 3D circuit of SDRE. Each wire represents a “bus” of channel-up and channel-down. The inset remark that each SDRE consists of resistivity for channel-up, for channel-down and a spin-flip-scattering resistance between both channels. The large resistors denotes for interface resistivity [Eq. (8)].

Although the construction of the  $\mathbb{Q}$ -matrix as presented here may be tedious, it is rather direct to establish its construction numerically. When the equation  $\mathbb{Q}\mathbb{H} = \mathbb{F}$  is solved, values of  $\mu_{\uparrow/\downarrow}$ ,  $J_{\uparrow/\downarrow}$  for each SDRE are directly written in  $\mathbb{H}$ -vector; their profiles can be determined by step-by-step applying multiplication in Eqs.(14)(16) and (17)(18).

### A. Construction of 3D electric circuit

In the previous Section we have derived the formalism to calculate  $J_{\uparrow/\downarrow}$  and  $\mu_{\uparrow/\downarrow}$  in arbitrary electric circuit. In this Section, we explain, how to describe the whole nanostructure as a circuit of SDREs, as sketched in Fig. 3.

Each part of the nanostructure is divided into 3D rectangular grid, the circuit nodes positions being  $x_i$ ,  $y_j$ ,  $z_k$ . Then, a given SDRE, for example in the  $x$ -direction, has length  $L_i = (x_{i-1} + x_i)/2$  and cross-sectional area  $S_{jk} = y_j z_k$ . Due to this treatment, the grid does not need to be equally spaced, but just rectangular.

At the interface between two different materials, e.g. A and B (see Fig. 3), SDRE is described by  $\mathbf{K}_{A \rightarrow B}$  matrix consisting of three contributions  $\mathbf{K}_{A \rightarrow B} = \mathbf{K}_{A \rightarrow \text{int}} \mathbf{K}_{\text{int}} \mathbf{K}_{\text{int} \rightarrow B}$  [Eq. (16)]. The  $\mathbf{K}_{A \rightarrow \text{int}}$  is contribution from grid point (node) inside A material to the interface with (SDRE is now along the  $z$ -direction)  $L_k = z_{\text{int}} - z_{k-1}$  and  $S_{ij} = x_i y_j$ .  $\mathbf{K}_{\text{int}}$  is the interface resistivity matrix given by Eq.(8).  $\mathbf{K}_{\text{int} \rightarrow B}$  is contribution from the interface to the node in B material having  $L = z_k - z_{\text{int}}$  and  $S_{ij} = x_i y_j$ .

The electrical circuit network as described above describes correctly charge current. However, inside 3D (2D)

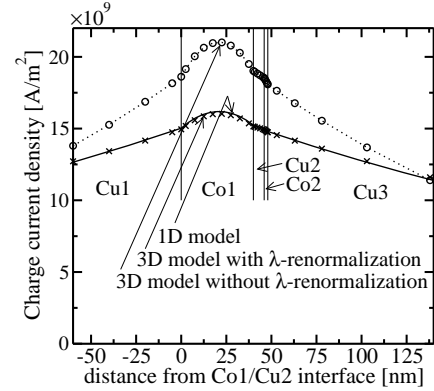


FIG. 4:  $j_{\text{sp}}$  through  $(\text{Cu}/\text{Co})^2$  structure with constant cross-sectional area  $S$  calculated by 1D model (line), by our 3D model with  $(\times)$  and without  $(\circ)$   $\lambda$ -renormalization.

SDRE circuit the volume of metal in all resistors is three (two) times larger than in reality. In such a case, the spin-polarized current would have larger dumping, as it would diffuse into larger volume. To correct this, it is necessary to calculate 1D propagation of  $\mu_{\uparrow/\downarrow}$  in each SDRE by slightly modified Eq. (1)

$$f \frac{\partial^2(\mu_{\uparrow} - \mu_{\downarrow})}{\partial x^2} = \frac{\mu_{\uparrow} - \mu_{\downarrow}}{\lambda^2}, \quad (25)$$

where  $f$  is a dimension of the SDRE circuit. In other words, when a given nanostructure is described by 3D (2D) electrical circuit, the  $\lambda$  should be increased by a factor  $\sqrt{3}$  ( $\sqrt{2}$ ). This  $\lambda$ -normalization should not be applied for open-end SDREs, as their contribution is correctly described by 1D propagation.

The advantage of this  $\lambda$ -normalization is shown in Figure 4, where  $j_{\text{sp}}$  through  $(\text{Cu}/\text{Co})^2$  structure (described and studied in detail in the next Section) is compared between 1D model (full line), and our 3D model without  $\lambda$ -normalization ( $\circ$ ) and with  $\lambda$ -normalization ( $\times$ ). We can see that with (without)  $\lambda$ -normalization, the agreement between 1D and 3D model is about 1% (30%). The same is valid for spin-accumulation  $\Delta\mu = \mu_{\uparrow} - \mu_{\downarrow}$ , where calculation without  $\lambda$ -normalization leads to 30% smaller  $\Delta\mu$ .

### B. Surface scattering

In this Section, we describe how to incorporate surface scattering to the presented formalism.

Surface scattering can be described by a shunting resistance  $R_s$  shortcircuiting up and down channels for a nodes situated just close to the wire surface.  $R_s$  has value  $R_{s,n} = AR_s/S_n$ ,  $AR_s$  being surface scattering resistivity and  $S_n$  being surface area corresponding to the  $n$ -th node. When surface scattering is not presented, then obviously  $R_{s,n} = \text{inf}$ . Surface scattering can be described

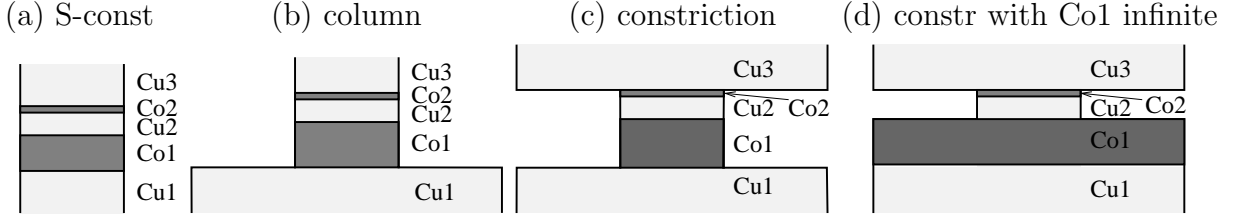


FIG. 5: Sketches of studied type structures. (a) S-constant (infinitely long nanowire with constant cross-section area  $S$ ), (b) column (infinitely long pillar deposited on infinitely large Cu1 layers) and (c) constriction (both Cu3 cover and Cu1 buffer layers are infinitely large) (d) constriction with Co1 infinite layer.

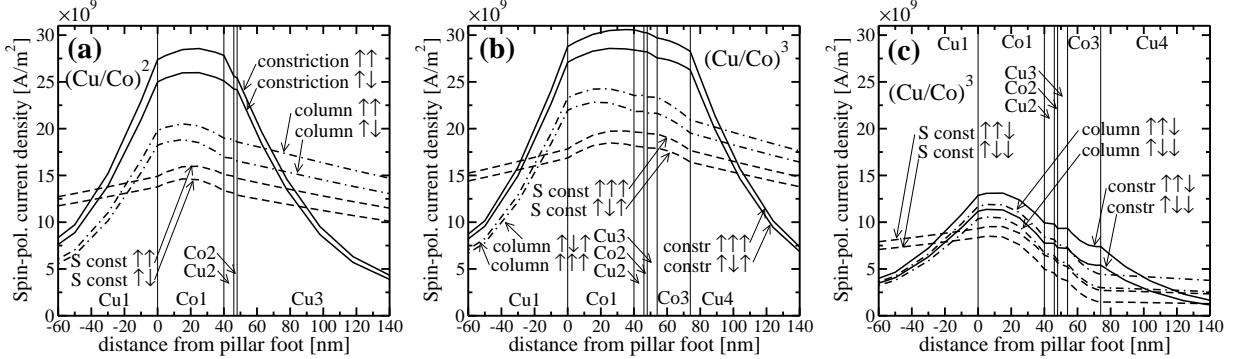


FIG. 6:  $j_{sp}$  along center axis of the (a)  $(Co/Cu)^2 \uparrow\uparrow, \uparrow\downarrow$  (b)  $(Co/Cu)^3 \uparrow\uparrow\uparrow, \uparrow\uparrow\downarrow$  (c)  $(Co/Cu)^3 \uparrow\uparrow\downarrow, \uparrow\downarrow\downarrow$  for S-constant, column and constriction structure types [Fig. 5].

by modification of Kirchoff law [Eq. (20)]

$$\sum_{k_n} J_{n,\uparrow/\downarrow}^{[k_n]} \mp \frac{\mu_{n,\uparrow} - \mu_{n,\downarrow}}{R_s} = 0. \quad (26)$$

To incorporate this modification into  $\mathbb{Q}$ -matrix for the  $n$ -th node, we add  $\mathbf{G}_s$  matrix

$$\mathbf{G}_s = \frac{1}{R_s} \begin{bmatrix} -1 & 1 \\ 1 & -1 \end{bmatrix} \quad (27)$$

on the  $n$ -th double-column and  $n$ -th double-row in the last part of  $\mathbb{Q}$ -matrix which describes current conservation in each node. In our example given by Eq. (22) and Figure 2, to add  $R_s$  to  $n = 2$  node, we place  $\mathbf{G}_s$  to the 7-th double-row and 2-nd double-column into  $\mathbb{Q}$ -matrix.

#### IV. APPLICATION TO (Cu/Co) PILLAR STRUCTURE

In this Section we use the above developed formalism on  $(Cu/Co)^2$  and  $(Cu/Co)^3$  pillar structures. We will show how spin-polarized current density  $j_{sp} = j_{\uparrow} - j_{\downarrow}$  and electrochemical potential  $\mu_{\uparrow/\downarrow}$  vary differently between when whole structure is a pillar or only a part of the structure is a pillar attached to an infinitely large continuous layer. In the literature, pillars terminated with infinitely large continuous layers are commonly used [2, 3, 4, 25, 26].

We have studied structures consisting of 2 and 3 Co layers, called  $(Cu/Co)^2$ , and  $(Cu/Co)^3$  with dimensions in nm Cu1/Co1(40)/Cu2(6)/Co2(2)/Cu3 and Cu1/Co1(40)/Cu2(6)/Co2(2)/Cu3(6)/Co3(20)/Cu4, respectively. The square-shaped pillar 100 nm in size begins with the Co1/Cu2 interface. The considered structure types are defined in Fig. 5 as (a) cross-sectional area  $S$  constant, (b) column, (c) constriction and (d) constriction with infinite Co1 layer. In the following discussion, ‘‘constriction’’ corresponds to the case (c). The ‘‘infinite’’ homogeneous layers were approximated as a square pillar of 800 nm in size. The magnetization of Co1 layer is always fixed as ‘‘up’’ ( $\uparrow$ ), whereas magnetic orientations of other Co layers are varied. Note that in our diffusive transport calculations, the magnetization orientation with respect to the structure (e.g. in-plane or out-of-plane) do not play any role, but only mutual magnetization orientation (parallel or antiparallel) does play an important role. The charge current passing through structure is assumed to be  $J_{ch} = 1$  mA, equivalent to the averaged charge current density in the pillar  $j_{ch} = 100 \times 10^9$  A/m<sup>2</sup>. The electrical properties of materials are of room temperature [16, 27, 28]: electric conductivity  $\sigma_{Cu} = 4.81 \times 10^6 \Omega^{-1} m^{-1}$ ,  $\sigma_{Co} = 4.2 \times 10^6 \Omega^{-1} m^{-1}$ , spin-flip-lengths  $\lambda_{Cu} = 350$  nm,  $\lambda_{Co} = 60$  nm and Co spin bulk assymetry  $\gamma = 0.35$ . We assume no interface resistance and no interface and surface scattering. The SDRE grid size is 10 nm.

	$j_{sp}$ [ $10^9 \text{ A/m}^2$ ]	$\Delta\mu$ [meV]	MR [%]
$(\text{Cu}/\text{Co})^2 \uparrow\uparrow$ S-constant (+)	14.85 [14.93]	-0.223 [-0.220]	0.483 [0.485]
$(\text{Cu}/\text{Co})^2 \uparrow\uparrow$ column (□)	19.0 [19.8]	-0.267 [-0.276]	0.63 [0.66]
$(\text{Cu}/\text{Co})^2 \uparrow\uparrow$ constriction (◇)	29.4 [33.7]	-0.052 [-0.009]	1.01 [1.17]
$(\text{Cu}/\text{Co})^2 \uparrow\uparrow$ constr, Co1 infinite	28.7 [23.3]	-0.050 [0.001]	1.43 [2.48]
$(\text{Cu}/\text{Co})^3 \uparrow\uparrow\uparrow$ S-constant (×)	19.51 [19.67]	-0.078 [-0.077]	0.444 [0.448]
$(\text{Cu}/\text{Co})^3 \uparrow\uparrow\uparrow$ column (△)	23.6 [24.5]	-0.171 [-0.184]	0.55 [0.57]
$(\text{Cu}/\text{Co})^3 \uparrow\uparrow\uparrow$ constriction (▽)	31.0 [33.9]	-0.019 [-0.005]	0.74 [0.81]
$(\text{Cu}/\text{Co})^3 \uparrow\uparrow\downarrow$ S-constant (*)	5.94 [5.93]	-0.442 [-0.438]	0.116 [0.115]
$(\text{Cu}/\text{Co})^3 \uparrow\uparrow\downarrow$ column (▷)	8.08 [8.49]	-0.490 [-0.494]	0.162 [0.171]
$(\text{Cu}/\text{Co})^3 \uparrow\uparrow\downarrow$ constriction (◁)	9.7 [10.5]	-0.458 [-0.456]	0.192 [0.210]

TABLE I: Values of  $j_{sp}$ ,  $\Delta\mu = \mu_\uparrow - \mu_\downarrow$  at the position of free Co2 layer for  $(\text{Cu}/\text{Co})^2$  and  $(\text{Cu}/\text{Co})^3$  structures. Magnetoresistance (MR) is determined between first and last Co/Cu interface. All values are determined as average over whole pillar cross-section area. In square brackets we present values calculated from modified 1D VF formalism, which takes into account a variable cross-sectional area of the layers (Sect. V). Symbols in parentheses denote structure notation in Fig. 11.

### A. Current density in the structure

Figure 6 shows the profile of  $j_{sp}$  along center axis of the structures: (a)  $(\text{Cu}/\text{Co})^2$  (b)  $(\text{Cu}/\text{Co})^3$  with parallel Co1 and Co3 layers and (c)  $(\text{Cu}/\text{Co})^3$  with antiparallel Co1 and Co3 layers for S constant, column and constriction type structures. In all cases,  $j_{sp}$  for parallel Co1 and Co3 layer is larger than for antiparallel configuration. Furthermore,  $j_{sp}$  is enhanced at the position of free Co2 layer for the column and constriction types compared to the S constant type structure. For example, in the case of the constriction type structure with  $(\text{Cu}/\text{Co})^2 \uparrow\uparrow$  configuration,  $j_{sp}$  is enhanced by a factor of 1.75 and in the case of  $(\text{Cu}/\text{Co})^3 \uparrow\uparrow\uparrow$  by 1.5. When only Cu buffer layer is infinite in size (column-type structure),  $j_{sp}$  at the position of Co2 layer is enhanced too, but not so strongly. Figure 6(c) shows that for  $(\text{Cu}/\text{Co})^3$  with antiparallel Co1 and Co3 layers,  $j_{sp}$  is significantly reduced for all types of structures.

The origin of the  $j_{sp}$  enhancement is following: the pillar is attached to infinitely large Cu layer which provides large volume for spin-current to be scattered and so acting as a strong spin-flip-scatterer. Hence, infinitely large Cu layer works as a small shortcircuiting resistance between up and down channels. Consequently, shortcircuiting of up and down channels leads to an increase in  $j_{sp}$ . The increase of  $j_{sp}$  is related with increase of spin-polarization efficiency  $p = j_{sp}(J_{ch}/S_{\text{pillar}})$ , as charge current flowing through pillar  $J_{ch}$  is fixed in all our calculations. Consequently, increase of  $p$  leads to decrease of critical switching current  $J_{s,ch}$  which is necessary to reverse magnetization direction of free layer.

As the constriction type structure is in the most common use for Co/Cu pillar structures, the  $j_{sp}$  enhancement (i.e.  $J_{s,ch}$  reduction) has been already widely used [4, 5] without being noticed. Similar effect can be realized by inserting a layer with small characteristic spin-flip resis-

tance  $AR_\lambda = \lambda/\sigma$ , such as Pt, Ag, Au, Ru above the last Co layer or bellow the first Co layer. Such cover layers has been used [29, 30] since the first pioneering experiment [3], but their contributions to the  $j_{sp}$  enhancement have been observed recently [30, 31, 32].

Figure 7 shows profiles of charge current  $j_{ch} = j_\uparrow + j_\downarrow$  along the center axis of the  $(\text{Cu}/\text{Co})^3$  structure for S constant, column and constriction type structures. Obviously, for S constant structure, the  $j_{ch}$  is constant. In the case of infinite Cu termination,  $j_{sp}$  decreases approximately exponentially over the characteristic length of 50 nm. The same decay of  $j_{sp}$  is presented in Fig. 6 for infinitely large Cu layers.

In Table I, we summarize averaged values of  $j_{sp}$  in the position of Co2 layer in all the types of studied structures. These  $j_{sp}$  values may differ from those presented in Fig. 6 due to lateral inhomogeneity of  $j_{sp}$  inside pillar, discussed in next Section. The largest averaged  $j_{sp}$  is obtained for  $(\text{Cu}/\text{Co})^3 \uparrow\uparrow\uparrow$  constriction structure ( $31.0 \times 10^9 \text{ A/m}^2$ ) and  $(\text{Cu}/\text{Co})^2 \uparrow\uparrow$  constriction struc-

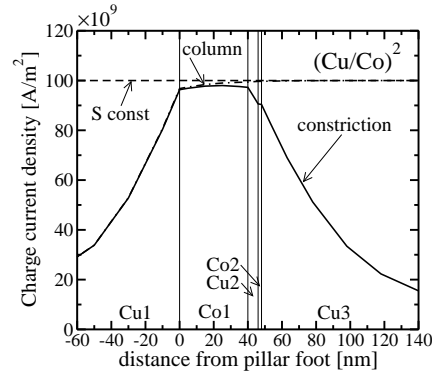


FIG. 7:  $j_{ch}$  along center axis of the  $(\text{Co}/\text{Cu})^2$  structure for S-constant, column and constriction structure types [Fig. 5].

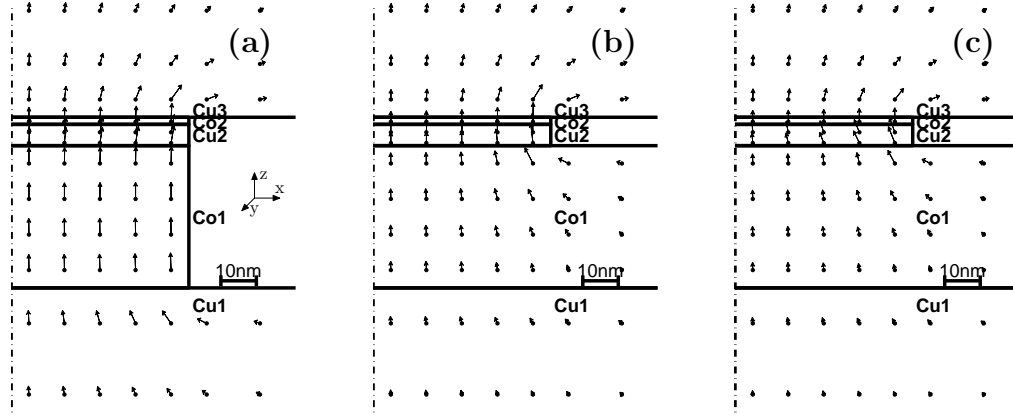


FIG. 8: Spin polarized current in  $(\text{Cu}/\text{Co})^2$  constriction-type structure (a) without infinitely large Co1 layer,  $\uparrow\uparrow$  (b) with infinitely large Co1 layer  $\uparrow\uparrow$  (c) as (b) but  $\uparrow\downarrow$ .

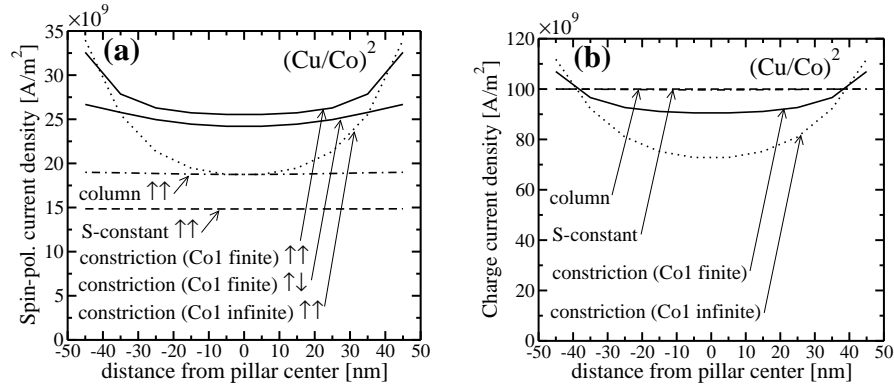


FIG. 9: (a)  $j_{\text{sp}}$  and (b)  $j_{\text{ch}}$  in the middle of the Co2 layer inside  $(\text{Cu}/\text{Co})^2$  structures.

ture ( $29.4 \times 10^9 \text{ A/m}^2$ ), providing  $j_{\text{sp}}$  enhancement by a factor 2 with respect to  $(\text{Co}/\text{Cu})^2$  S-constant structure ( $14.85 \times 10^9 \text{ A/m}^2$ ). This tendency is already explained in above paragraph.

### B. Current inhomogeneity inside pillar

Figure 8 presents a map of spin-polarized current density  $j_{\text{sp}}$  inside  $(\text{Cu}/\text{Co})^2$  constriction type structure for (a)(b) parallel and (c) antiparallel magnetization configuration. The case (a) is a structure without infinitely large Co1 layer whereas (b)(c) with it. A map of  $j_{\text{ch}}$  is not presented here as it looks similar to  $j_{\text{sp}}$  with  $\uparrow\uparrow$ . The  $j_{\text{sp}}$  inside Co2 layers is more homogenous and flows well perpendicular to the interfaces although in the surrounding Cu layers the  $j_{\text{sp}}$  can have rather large inclination and inhomogeneity. The  $j_{\text{sp}}$  tends to be more homogeneous when passing Co layer, causing that the  $j_{\text{sp}}$  in the adjacent Cu layers can have rather large in-plane components. This is remarkable in the case (c). Very similar tendency is found for  $j_{\text{ch}}$ .

The above mentioned characteristics of  $j_{\text{sp}}$  are consequence of larger spin-flip resistance  $AR_{\lambda} =$

$\lambda/\sigma$  of Co with respect to Cu,  $AR_{\lambda, \text{Co}} = 14.3 \text{ f}\Omega\text{m}^2$ ,  $AR_{\lambda, \text{Cu}} = 7.3 \text{ f}\Omega\text{m}^2$ . It means that spin-flip is more likely to occur inside Cu than inside Co. In other words, Co is “harder” material than Cu for  $j_{\text{sp}}$  to penetrate into it. The above mentioned characteristics of  $j_{\text{ch}}$  are simply consequence of  $\sigma_{\text{Co}} \ll \sigma_{\text{Cu}}$ .

Figure 9 shows cross-sectional (in  $x$ -direction) profiles of (a)  $j_{\text{sp}}$  and (b)  $j_{\text{ch}}$  through pillar in the middle of the Co2 layer for  $(\text{Cu}/\text{Co})^2$  structure. Both  $j_{\text{sp}}$  and  $j_{\text{ch}}$  are inhomogenous having minima at the structure center. This is due to inhomogenous current injection into the pillar from infinitely large layers. There is no  $j_{\text{sp}}$  and  $j_{\text{ch}}$  inhomogeneity for S constant and nearly no inhomogeneity in case of column type structure as the  $j_{\text{sp}}$  and  $j_{\text{ch}}$  are homogenized by a Co1 layer. For constriction type structure the inhomogeneity is 12% for  $\uparrow\uparrow$  and 5% for  $\uparrow\downarrow$ . Inhomogeneity is defined as  $(j_{\text{max}} - j_{\text{min}})/(j_{\text{max}} + j_{\text{min}})$ , where maximal, minimal value is taken from cross-sectional current distribution in Fig. 9. The inhomogeneity is reduced for  $\uparrow\downarrow$  due to different conductivities of up and down channel conductivities, leading to other current homogenization in Cu2 spacer layer. If Co1 layer is infinitely large, the inhomogeneity is increased to 10% and 29% for  $\uparrow\uparrow$  and  $\uparrow\downarrow$ , respectively. The  $j_{\text{ch}}$  inhomogeneity is 8% and

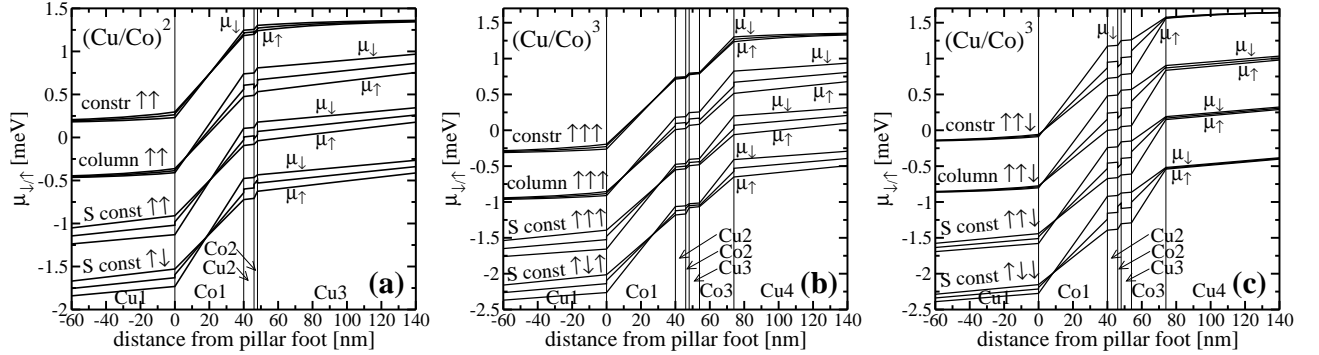


FIG. 10: Electro-chemical potential  $\mu_{\uparrow/\downarrow}$  along center axis of the (a)  $(\text{Cu}/\text{Co})^2$   $\uparrow\uparrow$ ,  $\uparrow\downarrow$  (b)  $(\text{Cu}/\text{Co})^3$   $\uparrow\uparrow\uparrow$ ,  $\uparrow\downarrow\uparrow$  and (c)  $(\text{Cu}/\text{Co})^3$   $\uparrow\uparrow\downarrow\downarrow$ ,  $\uparrow\downarrow\downarrow\downarrow$  for S constant, column and constriction structure types [Fig. 5].

20% for constriction type structure with and without infinitely large Co1 layer, respectively.

Here remains a question whether such a  $j_{sp}$  inhomogeneities make current magnetization reversal easier or not. Advantage of  $j_{sp}$  inhomogeneity may be, that it locally enhanced  $j_{sp}$  near the pillar edge, whereas decreasing  $j_{sp}$  at the pillar center. As shown in Table I, the mean value of  $j_{sp}$  is about the same for  $(\text{Cu}/\text{Co})^2$  constriction structure with and without infinitely large Co1 layer. However, in the second case,  $j_{sp}$  is much more inhomogeneous. This is not well presented in Fig. 9(a), we do not see the largest  $j_{sp}$  flowing in the vicinity of the corners of the square pillars. Disadvantage of  $j_{sp}$  inhomogeneity may be different magnitude of torque exerted on magnetic spins of free Co2 layer. This may be particularly important in the case of high speed switching associated with magnetization precession.

### C. Electrochemical potential inside structure

Figure 10 presents profiles of  $\mu_{\uparrow}$ ,  $\mu_{\downarrow}$  and  $\tilde{\mu}$  (hereafter  $\mu$ -profiles) along the center axis of the (a)  $(\text{Cu}/\text{Co})^2$   $\uparrow\uparrow$ ,  $\uparrow\downarrow$  (b)  $(\text{Cu}/\text{Co})^3$   $\uparrow\uparrow\uparrow$ ,  $\uparrow\downarrow\uparrow$  and (c)  $(\text{Cu}/\text{Co})^3$   $\uparrow\uparrow\downarrow\downarrow$ ,  $\uparrow\downarrow\downarrow\downarrow$ . S-constant structure is presented for both magnetization directions of Co2 layers, although column and constriction types are presented only for  $\uparrow$  magnetization of Co2 layer. In contrast to  $j_{sp}$ , inhomogeneity of spin accumulation  $\Delta\mu$  at the position of free Co2 layer is very small, mostly below 1%. Table I presents a mean value of  $\Delta\mu$  for all types of the studied structures.

Figures 10 (a)(b) and (c) show that  $\mu$ -profiles depend slightly on magnetization of free Co2 layer because  $t_{\text{Co}2} \ll \lambda_{\text{Co}}$ . Figure 10(a) exhibits suppression of  $\Delta\mu$  in the vicinity of infinitely large Cu layer. The reason is exactly the same as discussed in Sec. IV A: the infinitely large Cu layer works as a strong spin-scatterer, causing a small spin-flip resistance (large scattering) between up and down channels. Obviously, such a shortcut reduces  $\Delta\mu$ .

This is contradictory to [30, 31, 32], where it is argued that presence of spin-scatterer increases spin accumulation

$\Delta\mu$  inside pillar. It should be emphasized that presence of spin-scatterers increases  $j_{sp}$  (and magnetoresistance) in the pillar, but *reduce*  $\Delta\mu$ .

Table I shows that the largest  $\Delta\mu$  is obtained for column type structure, by 20% larger than for S-constant type structure. The reason is as follows: when Cu1 is not infinitely large (S constant structure),  $\Delta\mu$  changes its sign approximately in the middle of Co1 layer [Fig. 10(a) S constant]. When Cu1 is infinitely large, it acts as strong spin-scatterer and shortcuts up and down channels. Hence,  $\Delta\mu$  at Cu1/Co1 interface is nearly zero and hence larger  $\Delta\mu$  is obtained at the Co1/Cu2 interface and inside Co2 layer [Fig. 10(a) column]. But to realize this, it is necessary that up and down channels above free Co2 layer should not be shortcut meaning that the cover layer has not to be infinite.

Figure 10(b) shows that  $\Delta\mu$  is reduced when Co1 and Co3 layers have parallel magnetization configuration. Figure 10(c) shows an increase in  $\Delta\mu$  when Co1 and Co3 layers are antiparallel, enhancing  $\Delta\mu$  by a factor of 2 with respect to  $(\text{Cu}/\text{Co})^2$  S constant structure. In this case the types of structure are not so important as in  $(\text{Cu}/\text{Co})^2$  case, because  $\Delta\mu$  at the position of Co2 free layer is “screened” by spin-scattering inside Co1 and Co3 layers.

Hence, there is effectively no spin-accumulation  $\Delta\mu$  in the case of a commonly used constriction type structure with two FM layers. It may explain why this contribution to magnetization reversal (predicted in [33]) was not observed in Co/Cu structure [25]. To obtain non-zero  $\Delta\mu$ , it is necessary to use either 3 FM layer system with antiparallel configuration of first and last FM layers, or to ensure that structure above free layer will not contain spin-scatterers. It can be reached when pillar structure above free layer (i) does not contain any strong spin-scatterer layers (as Au, Ag, Pt, Ru) and (ii) the cover layer does not contain large volume of metal. It means that pillar current drain should be realized by a long pillar or by a thin cover layer.

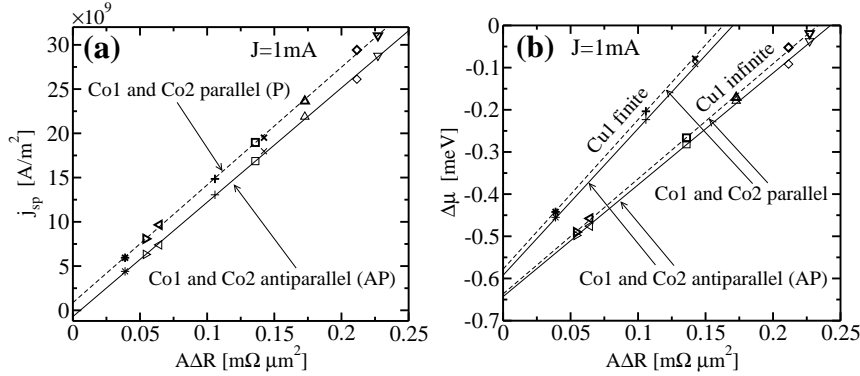


FIG. 11: Dependence of (a)  $j_{sp}$  and (b)  $\Delta\mu$  on  $A\Delta R$  for different studied (Cu/Co) structure, symbol notation in Tab I. Lines are the best linear fits, dashed line and bold symbols (full line and normal symbols) denote parallel (antiparallel) Co1 and Co2 layers. Cu1 infinite means column and constriction types, Cu1 finite means S constant type.

#### D. Magnetoresistance

Finally, we discuss influence of type structure on magnetoresistance ratio (MR), presented in the last column in Table I. The value of MR is determined as  $MR = (\Delta\tilde{\mu}_\uparrow - \Delta\tilde{\mu}_\downarrow)/(\Delta\tilde{\mu}_\uparrow + \Delta\tilde{\mu}_\downarrow)$ , where  $\uparrow, \downarrow$  denotes magnetization of free Co2 layer,  $\Delta\tilde{\mu}_{\uparrow/\downarrow} = \tilde{\mu}_{last,\uparrow/\downarrow} - \tilde{\mu}_{first,\uparrow/\downarrow}$ , where  $\tilde{\mu}_{first,\uparrow/\downarrow}$  and  $\tilde{\mu}_{last,\uparrow/\downarrow}$  are determined on Cu side of the first and last Cu/Co interface, respectively.

The calculated value of MR in the case of (Cu/Co)<sup>2</sup> S-constant structure is 0.48%. However, in the case of (Cu/Co)<sup>2</sup> constriction type, it reaches 1.01% (enhancement by a factor of 2) and in the case of the constriction with infinite Co1 layer even 1.43% (enhancement by a factor of 3). The last value may be misleading as this increase is mainly due to resistivity reduction of Co1 infinite layer.

Table I shows MR is strongly affected by the type structure, increasing with an increase of  $j_{sp}$  rather than  $\Delta\mu$ . This tendency may be observed also for (Co/Cu)<sup>3</sup> layer, showing increase (decrease) in MR when Co1 and Co3 layers have parallel (antiparallel) magnetization configuration.

Figure 11(a) shows dependence of  $j_{sp}$  on  $A\Delta R$ , where  $\Delta R = R_\uparrow - R_\downarrow$ , where  $\uparrow, \downarrow$  means up, down magnetization of Co2 layer, respectively. It shows that  $j_{sp}$  is proportional to  $\Delta R$ . This figure is analogous to the experimental dependence of critical switching current  $J_{s,ch}$  as a function of  $\Delta R$  [30, 31, 32], where they found that  $1/J_{s,ch}$  is proportional to  $\Delta R$ .

These graphs are analogous from following reasons: to switch magnetic layer we need to overcome the critical spin-polarized current density

$$j_{s,sp,0} = pJ_{s,ch}/S_{pillar}, \quad (28)$$

where  $J_{s,ch}$  is critical switching charge current and  $p$  is spin-polarized current injection efficiency. Because  $j_{s,sp,0}$  and  $S_{pillar}$  are constant, so  $p \sim 1/J_{s,ch}$ . On the other hand, from our calculations, we can express  $p$  as  $p = j_{sp}/(J_{ch}/S_{pillar})$ , where  $J_{ch}$  is a fixed charge current

flowing to the structure; therefore  $p \sim j_{sp}$ . However, in our model,  $j_{sp}$  is slightly larger for Co1 and Co2 parallel configuration (Fig. 6), although in [30, 31, 32],  $1/J_{s,ch}$  is larger for antiparallel configuration, in agreement with the spin-transfer model [34]. Figure 11(a) also provides an important consequence: when changing electric properties of surroundings of FM(fixed)/spacer/FM(free) layers, an enhancement of  $j_{sp}$  in the position of free layer leads to enhancement of MR.

Figure 11(b) shows dependence of  $\Delta\mu$  on  $\Delta R$ . We can see that with increasing  $\Delta R$ ,  $\Delta\mu$  is reduced. Two different slopes correspond to two different “sources”  $\Delta\mu$  acting as with different “hardness”. The source hardness is determined by a presence or absence of scatterers bellow fixed Co1 layer. Hard source is for constriction and column structure type, i.e. when Cu1 is infinitely large. Weak one is for S constant structure type, i.e. when for Cu1 is not infinitely large. The explanation of this behavior has been already provided in previous Section IV C: when spin-flip scatterer is presented bellow fixed Co1 layer, it vanishes  $\Delta\mu$  on Cu1/Co1 interface and hence provides harder source of  $\Delta\mu$ . Figure 11 also shows that when changing surroundings of FM(fixed)/spacer/FM(free) layers, an increase in  $\Delta\mu$  at the position of free layer is related to a decrease of MR.

Remark, that for constriction type structure with Co1 layer infinitely large [case(d) in Fig. 5], the “source” of  $\Delta\mu$  becomes softer than for constriction type [case (c) in Fig. 5].

#### V. EXPRESSION OF INFINITELY LARGE LAYERS BY 1D MODELS

As we have shown, the constriction type structures modify the profile of both  $j_{sp}$  and  $\mu_{\uparrow/\downarrow}$  with respect to S constant types, which provides equivalent results to 1D VF formalism [11]. However, to describe  $j_{sp}$  and  $\mu_{\uparrow/\downarrow}$  inside structure by 3D model may be tedious procedure. That is why here we discuss briefly, how to modified VF

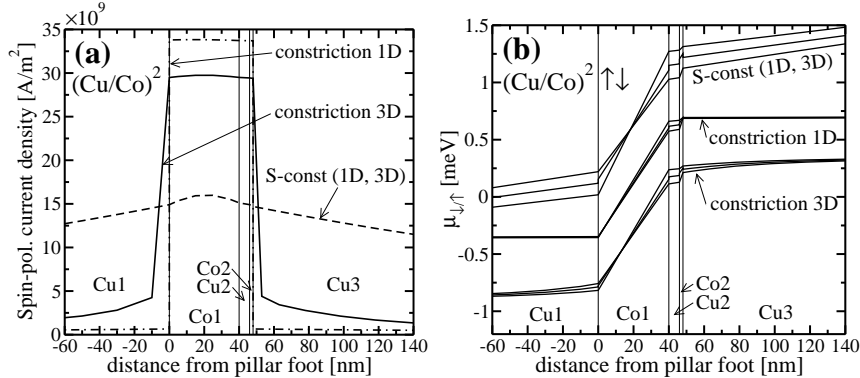


FIG. 12: (a) averaged value of spin-polarized current and (b)  $\mu_{\uparrow/\downarrow}$  in the structure center calculated for constriction type structure with and without Co1 infinite layer in the  $(\text{Cu}/\text{Co})^2 \uparrow \downarrow$  compared with 1D calculations taking into account infinite Cu layers. See Section V for detail.

model to take into account infinitely large layers.

We propose, that each layer can have its own cross-sectional area  $S_i$ . Then, instead of conserving spin polarized current density  $j_{\uparrow/\downarrow}$  in the 1D formalism, we propose to conserve spin polarized current  $J_{\uparrow/\downarrow}$ . Actually, we have used this boundary condition already in Section II B. This boundary condition is justified when (i) thickness of the layer  $L_i$  is thick enough compared to the change of pillar diameter between neighboring layers,  $|a_{i+1} - a_i| < L_i$ ,  $|a_i - a_{i-1}| < L_i$ , where  $a_i \approx \sqrt{S_i}$ , so that current has enough space to spread to different cross-sectional area  $S_i$  (ii) pillar diameter  $a_i$  is smaller than spin-flip length  $\lambda$ . It can be shown that if  $S_i \rightarrow \text{inf}$ , then  $j_{\uparrow/\downarrow}$ ,  $\mu_{\uparrow/\downarrow}$ , MR etc. converge. So, it is not important, how large value  $S_i$  is used to describe infinitely large layers.

Figure 12 shows  $j_{sp}$  and  $\mu_{\uparrow/\downarrow}$  calculated by 3D models in the case of constriction type structure. These data are compared with 1D models with and without expanding the terminating Cu layers, called “1D constriction” and “S constant”, respectively.

3D constriction is described by 1D constriction (S constant) model with precision of 15% (50%) for  $j_{sp}$  and 40% (80%) for  $\Delta\mu$  [Fig. 12(a)(b)]. The agreement between  $\Delta\mu$  for constriction type structure is quite poor, because  $\Delta\mu$  at this configuration is very small. In the case of  $\Delta\mu$  larger than the above case, the agreement is about 10%.

This 1D model has been used to calculate  $j_{sp}$ ,  $\Delta\mu$  and MR in the position of free Co2 layer for all types of studied structures. The results are presented in Table I in square brackets; we can see rather good agreement in all cases. An exception is the case of constriction type structure with infinitely large Co1 layer, as in this case the condition (ii) is not fulfilled.

## VI. CONCLUSION

We have developed formalism which allows to calculate spin-polarized current  $j_{sp}$ , and electrochemical potential  $\mu_{\uparrow/\downarrow}$  inside arbitrary electric circuit, consisting of ferro- or non-magnetic metallic SDRE elements as well as interface and surface resistivities. The formalism is limited to the parallel/antiparallel magnetic orientation in diffusive regime.

To calculate spatial distribution of  $\mu_{\uparrow/\downarrow}$ ,  $j_{\uparrow/\downarrow}$  inside nanostructure, we divide the structure into an 1D, 2D or 3D electric circuit network of SDRE elements which is successively solved. When division is carried out as described in Section III A, the renormalization of spin-flip length  $\lambda$  has to be performed.

This formalism is applied to  $(\text{Cu}/\text{Co})^2$  and  $(\text{Cu}/\text{Co})^3$ , pillar structures, where pillar cross-sectional area of starting/terminating layers were assumed to be either infinitely large (column type, constriction type) or they have the same cross-sectional area as pillar (S const types).

Inside the pillar surrounded by infinitely large layers, the  $j_{sp}$ ,  $j_{ch}$  can be inhomogeneous. Maximal inhomogeneity is found to be 29% and 20% in the case of infinitely large Co1 layer. On the other hand, profile of  $\Delta\mu$  is found more homogeneous, with found maximum inhomogeneity of 2%. Such  $j_{sp}$  inhomogeneities may locally enhance the value of  $j_{sp}$ , but they may disturb the magnetization reversal associated with spin precession. Due to  $\sigma_{\text{Co}} \ll \sigma_{\text{Cu}}$ ,  $AR_{\lambda, \text{Co}} \gg AR_{\lambda, \text{Cu}}$ , both  $j_{ch}$  and  $j_{sp}$  flow rather perpendicular to the Co layers and furthermore the presence of Co layer makes  $j_{sp}$ ,  $j_{ch}$  more homogeneous.

When pillar is terminated by infinitely large layers, they serve as spin-scatterers, shortcircuiting up and down channels and hence modifying profiles of  $\Delta\mu$  and  $j_{sp}$ .

When such a spin-scatterers (but it is also valid for different spin-scatterers, as layers of Au, Ag, Pt, Ru, etc.) are introduced bellow “fixed” Co1 layer, they make  $\Delta\mu$  source “harder”. When they are placed above free Co2

layer, they shortcut up and down channels, reducing  $\Delta\mu$  nearly to zero, and hence enhancing  $j_{sp}$ .

Consequently, to get maximum  $j_{sp}$  in the case of  $(\text{Cu}/\text{Co})^2$  at the position of “free” Co2 layer, it is important to introduce spin-scatterers both bellow fixed Co1 layer and above free Co2 layer. To get maximum  $\Delta\mu$ , it is important to introduce spin-scatterer bellow fixed Co1 layer, but reduce spin-scattering above Co2 free layer, latter one can be realized by reducing volume of material above Co2 layer, for example current drain can be thin long nanowire or cover layer with very thin thickness. As most of experimentally studied  $(\text{Cu}/\text{Co})^2$  structures have infinitely large layers at both ends,  $\Delta\mu$  inside them is nearly zero.

For  $(\text{Cu}/\text{Co})^3$  system, maximum  $j_{sp}$  ( $\Delta\mu$ ) is for parallel (antiparallel) magnetization of first, last Co layer. When applying above described optimizations,  $j_{sp}$  and  $\Delta\mu$  can be further enhanced.

Furthermore, in agreement with experimental results [30, 31, 32] we found that  $j_{sp}$  is linearly proportional to  $\Delta R = R_\downarrow - R_\uparrow$  (and hence MR is increased when increasing  $j_{sp}$  at the position of free Co2 layer). Furthermore, dependence of  $\Delta\mu(\Delta R)$  is also linear, but  $\Delta\mu$  is reduced when increasing  $\Delta R$  (when increasing MR).

Finally, we propose simple modification of 1D Valet-Fert formalism [11], to incorporate spin-scattering induced by infinitely large layers attached to pillar.

---

[1] J.-E. Wegrowe, D. Kelly, Y. Jaccard, Ph. Guittienne, and J.-Ph. Ansermet, *Europhys. Lett.* **45**, 626 (1999).

[2] F. J. Albert, J. A. Katine, R. A. Buhrman, and D. C. Ralph, *Appl. Phys. Lett.* **77**, 3809 (2000).

[3] J. A. Katine, F. J. Albert, R. A. Buhrman, E. B. Myers, and D. C. Ralph, *Phys. Rev. Lett.* **84**, 3149 (2000).

[4] J. Z. Sun *et al.*, *J. Appl. Phys.* **93**, 6859 (2003).

[5] B. Özyilmaz *et al.*, *Phys. Rev. Lett.* **91**, 067203 (2003).

[6] T. Y. Chen, Y. Ji, C. L. Chien, and M. D. Stiles, *Phys. Rev. Lett.* **93**, 026601 (2004).

[7] A. Fábián *et al.*, *Phys. Rev. Lett.* **91**, 257209 (2003).

[8] B. Engel *et al.*, *Nanotechnology, IEEE Transactions on* **1**, 32 (2002).

[9] M. Johnson, *Science* **260**, 320 (1993).

[10] A. Brataas, Y. Tserkovnyak, G. E. W. Bauer, and B. I. Halperin, *Phys. Rev. B* **66**, 060404R (2002).

[11] T. Valet and A. Fert, *Phys. Rev. B* **48**, 7099 (1993).

[12] A. Brataas, Y. V. Nazarov, and G. E. W. Bauer, *Phys. Rev. Lett.* **84**, 2481 (2000).

[13] X. Waintal, E. B. Myers, P. W. Brouwer, and D. C. Ralph, *Phys. Rev. B* **62**, 12317 (2000).

[14] G. E. W. Bauer, Y. Tserkovnyak, D. Huertas-Hernando, and A. Brataas, *Phys. Rev. B* **67**, 094421 (2003).

[15] P. M. Levy and J. Zhang, *cond-mat/0405613*.

[16] F. J. Jedema, M. S. Nijboer, A. T. Filip, and B. J. van Wees, *Phys. Rev. B* **67**, 085319 (2003).

[17] F. Ernult *et al.*, *Eur. Phys. J. B* **25**, 177 (2002).

[18] M. Ichimura, S. Takahashi, K. Ito, and S. Maekawa, *J. Appl. Phys.* **95**, 7255 (2004).

[19] P. C. van Son, H. van Kempen, and P. Wyder, *Phys. Rev. Lett.* **58**, 2271 (1987).

[20] S. Takahashi and S. Maekawa, *Phys. Rev. B* **67**, 052409 (2003).

[21] P. Yeh, *Surf. Sci.* **96**, 625 (1980).

[22] Š. Višňovský, *Czech. J. Phys. B* **36**, 625 (1986).

[23] W. Park *et al.*, *Phys. Rev. B* **62**, 1178 (2000).

[24] C. H. Marrows and B. J. Hickey, *Phys. Rev. B* **63**, 220405(R) (2001).

[25] F. J. Albert, N. C. Emley, E. B. Myers, D. C. Ralph, and R. A. Buhrman, *Phys. Rev. Lett.* **89**, 226802 (2002).

[26] J. Grollier *et al.*, *Phys. Rev. B* **67**, 174402 (2003).

[27] S. K. Upadhyay, A. Palanisami, R. N. Louie, and R. A. Buhrman, *Phys. Rev. Lett.* **81**, 3247 (1998).

[28] L. Piraux, S. Dubois, A. Fert, and L. Belliard, *Eur. Phys. J. B* **4**, 413 (1998).

[29] N. C. Emley *et al.*, *Appl. Phys. Lett.* **84**, 4257 (2004).

[30] Y. Jiang *et al.*, *Phys. Rev. Lett.* **92**, 167204 (2004).

[31] S. Urazhdin, N. O. Birge, W. P. Pratt Jr., and J. Bass, *cond-mat/0312287*.

[32] S. Urazhdin, N. O. Birge, W. P. Pratt Jr., and J. Bass, *cond-mat/0309191*.

[33] C. Heide, P. E. Zilberman, and R. J. Elliott, *Phys. Rev. B* **63**, 064424 (2001).

[34] J. Slonczewski, *J. Magn. Magn. Mater.* **159**, 9353 (1996).